Research Article Vol. 13, No. 4 / 1 Apr 2022 / Biomedical Optics Express 1995
Biomedical Optics EXPRESS

Noninvasive assessment of liver function reserve with fluorescent dosimetry of indocyanine green

PEI-CHUN WU,[1,2,3,14] LUN-ZHANG GUO,[2,14] SHAN YU,[1,4,14] NING ZENG,[5,6,14] YU-CHENG LIU,[1] JIA YU,[1] ZHIMING ZHANG,[1] KE LU,[1] LIANGYU SUN,[1] CHUNFEI WANG,[1] YU-HAN CHANG,[2,3] YIN-LIN LU,[1,3] YU-FANG SHEN,[7,8] SHENG TAI,[9] YUEH-HSUN CHUANG,[10] JA-AN ANNIE HO,[11] KAI-WEN HUANG,[12] YAO-MING WU,[13] AND TZU-MING LIU[1,*]

[1]*Institute of Translational Medicine, Faculty of Health Sciences & Ministry of Education Frontiers Science Center for Precision Oncology, University of Macau, Taipa, Macau, China*
[2]*Department of Biomedical Engineering, National Taiwan University, Taipei 10617, Taiwan*
[3]*Molecular Imaging Center, National Taiwan University, Taipei 10617, Taiwan*
[4]*Department of Pathology, The Secondary Affiliated Hospital of Harbin Medical University, Harbin 150080, China*
[5]*First Department of Hepatobiliary Surgery, Zhujiang Hospital, Southern Medical University, Guangzhou 510280, China*
[6]*Guangdong Provincial Clinical and Engineering Technology Center of Digital Medicine, Guangzhou 510280, China*
[7]*3D Printing Medical Research Institute, Asia University, Taichung 41354, Taiwan*
[8]*Department of Bioinformatics and Medical Engineering, Asia University, Taichung 41354, Taiwan*
[9]*Department of Hepatopancreatobiliary Surgery, The Secondary Affiliated Hospital of Harbin Medical University, Harbin 150080, China*
[10]*Department of Anesthesiology, National Taiwan University Hospital, Taipei 10002, Taiwan*
[11]*Bioanalytical Chemistry and Nanobiomedicine Laboratory, Department of Biochemical Science & Technology, National Taiwan University, Taipei 10617, Taiwan*
[12]*Graduate Institute of Clinical Medicine, National Taiwan University College of Medicine, Taipei 10002, Taiwan*
[13]*Department of Surgery, National Taiwan University Hospital and College of Medicine, Taipei 10002, Taiwan*
[14]*Contributed equally*
[*]*tmliu@um.edu.mo*

Abstract: Using *in vivo* multiphoton fluorescent dosimetry, we demonstrate that the clearance dynamics of Indocyanine Green (ICG) in the blood can quickly reveal liver function reserve. In normal rats, the ICG retention rate was below 10% at the 15-minute post-administration; While in the rat with severe hepatocellular carcinoma (HCC), the 15-minute retention rate is over 40% due to poor liver metabolism. With a 785 nm CW laser, the fluorescence dosimeter can evaluate the liver function reserve at a 1/10 clinical dosage of ICG without any blood sampling. In the future, this low-dosage ICG 15-minute retention dosimetry can be applied for the preoperative assessment of hepatectomy or timely perioperative examination.

1. Introduction

Hepatocellular carcinoma (HCC) is one of the mortal malignancies with poor clinical treatment outcomes worldwide [1]. Liver resection is the major treatment option to prolong the living of an HCC patient [2]. However, sufficient metabolic function of the liver remnant is pivotal to

#446749 https://doi.org/10.1364/BOE.446749
Journal © 2022 Received 29 Oct 2021; revised 9 Feb 2022; accepted 10 Feb 2022; published 10 Mar 2022

Biomedical Optics EXPRESS

avoid postoperative liver failure. Insufficient liver function reserve will prohibit the possibility or restrict the extent of liver resection. Therefore, precise and accurate evaluation of the liver function reserve before the operation or during the surgery is crucial to increase the success rate of HCC hepatectomy. To mitigate the risk of postoperative liver malfunction, clinical scientists developed several methods, such as Child-Pugh score [3–6] and model for end-stage liver disease (MELD) score [5,6]. Child-Pugh's score has been well accepted for determining the prognosis of liver resection all over the world [3,4]. The assessments include the bilirubin level, albumin level, ascites, encephalopathy condition, and nutritional status. The resulting scores separate into A, B, and C levels, where Level C indicates more severe cirrhosis [5]. Although the Child-Pugh score is easy to measure, it cannot accurately reflect the actual function of the liver. Some patients with level A still have liver failure after surgery. Evidence indicates that these indices may oversimplify the representation of the liver function, and the score is not directly correlated with mortality rate [5]. The evaluations are, to some extent, subjective [6].

Medical imaging like computed tomography (CT) [7], magnetic resonance imaging (MRI) [8], and intraoperative ultrasound (IOUS) [9] provide structural information of HCC lesions, facilitating the estimation of cirrhosis volume. The reserved liver function can thus be linked to the non-cirrhosis volume of the liver [10]. However, the future remnant liver volume is not equivalent to future remnant liver function [11]. There is still no clear consensus on how much proportion of the liver could be removed according to these structural images. Therefore, there is an urgent demand to develop a functional assay that can complement the structural information of medical imaging and specifically reflect the liver functional reserve [11]. Jaundice is a molecular symptom of raised serum bilirubin caused by the decreasing metabolic function of the liver. Based on similar concepts, many liver-specific metabolic probes were developed to predict the functional reserve of the liver. Examples are ^{99m}Tc-IDA for hepatobiliary scintigraphy [12], and ^{99m}Tc labeled diethylene triamine pentaacetate-galactosyl hu-man serum albumin (^{99m}Tc-GSA) for SPECT/CT fusion imaging [13]. Although they can help the clinicians to understand the association between liver function and liver volume [14], the long duration of the drug uptake, the volume of equipment, the long testing time, and the radial hazard are still the major obstacles for a quick estimation.

In contrast, the indocyanine green (ICG) 15-minute retention test (ICG-R15) quantified by the infrared absorption has become the commonly used molecular assay in preoperative assessment of liver function [15]. The circulated ICG conjugated with proteins in blood is specifically metabolized through the liver into the bile duct [16]. The decay of ICG concentration in blood can thus reflect the liver metabolic function if well perfused. One traditional procedure of the ICG-R15 test is blood sampling at the 5th, 10th, 15th minutes post-ICG injection with a nontoxic dosage of 0.1–0.5 mg per kg body weight [17]. Then the ICG concentration in serum can be measured by spectrophotometry. The ICG-R15 in healthy people is typically less than 10%, but greater than 40% in patients with severe hepatic diseases [18]. One study reveals that ICG-R15 is more accurate than the Child-Pugh and MELD scores in predicting hepatic functional reserve before hepatectomy [19]. However, multiple blood drawings are invasive for patients and take time to quantify. Moreover, the preoperative ICG test assumes a constant baseline function without fluctuation, which might not reflect the worst situation in the course or after the surgery. If new satellite sites of HCC were found in operation, the reserved liver function can't be timely evaluated by the ICG-R15 test, and the resection volume can't be optimized [20].

To achieve continuous on-site measurement of ICG concentration in circulation, Nihon Kohden company has developed the pulse-dye-dosimetry (PDD) technique by measuring the absorption of ICG at 805 nm and heme at 890 nm [21,22]. The device is designed to evaluate cardiac output. But for the assay of ICG retention, the system needs to be sensitive enough to detect 1/100 of the initial bolus concentration so that 10% ICG-R15 can be confidently detected. At low ICG concentration, the absorption might be interfered with by skin pigment and the variation of

Biomedical Optics EXPRESS

hematocrit, which would affect the accuracy of measurement and causes a decrease of sensitivity in quantifying ICG. To address this issue, Dorshow *et al.* used the 820-850 nm fluorescence of ICG to achieve background-free quantification [23]. But the intended use for Dorshow's work still focuses on the evaluation of cardiac output. The dosage of ICG is 4-5 times higher than the clinically recommended dose (0.5 mg/kg). Overdosing will lead to the aggregation of ICG and reduce the quantum efficiency of the fluorescence emission [24]. The ICG-R15 retention rate would thus be overestimated. Tingting *et al.* used photoacoustic tomography to study the feasibility of ICG dosimetry in partial hepatectomy rabbits [25]. The animal model is still not in the context of HCC.

In this work, we investigate the low-dose ICG fluorescent dosimetry for the continuous evaluation of liver function in the HCC animal model. First, we used the *in vivo* multiphoton microscopy to analyze the liver functional reserve of HCC rats, and the ICG fluorescence decay in blood vessels supports the clinical criteria in the ICG-R15 test. Next, we used the 785 nm continuous wave (CW) laser system to achieve 1/10 clinical dose ICG fluorescence dosimeter for quick and portable liver function evaluation. In the future, this system could evaluate liver function multiple times in preoperative, intraoperative, or postoperative assessment.

2. Materials and methods

2.1. Harmonic generation and two-photon fluorescence imaging system

The laser-scanned inverted microscope system (Leica, DMI 3000M) was excited by a home-build 1250 nm femtosecond Cr: forsterite laser. Details about the light source and the imaging system have been reported elsewhere [25]. The mode-locked output power was 570 mW. The laser was scanned by a 16-kHz resonant mirror and a Galvo mirror. The beam size of the excitation light was expanded to fill the back aperture of an objective (Zeiss, 63×/1.15) to achieve the optimal resolution of the sectioning image. The generated multiphoton signals were epi-collected by the same objective and transmitted through the dichroic beam splitter with a 900 nm edge wavelength. The third harmonic generation (THG) signals ($\lambda = 417$ nm) and two-photon fluorescence (TPF) signals were further split by a 484 nm edge dichroic beam splitter and detected by two photomultiplier tubes (Hamamatsu, H7732-10) separately. To reject the background fluorescence and obtain better image contrast, we employed a 414 nm centered bandpass filter and a 650 nm edge long-pass filter before the corresponding detection channel. Pixel signal of images was digitally sampled, recorded, and assembled by a Field Programmable Gate Array card. The raster-scanned images were then displayed on the computer screen at a 30-Hz video rate. Each scanned image has an 80×80 μm field of view with 512×512 pixels. We used the THG image to locate the vessel and record the TPF of ICG as a multiphoton fluorescent dosimeter.

2.2. Fluorescent dosimeter with a 785 nm CW laser

The single-photon fluorescent dosimeter (Fig. 1) was composed of a 785-nm CW laser source (Coherent, OBIS785LX), a dichroic beam-splitting excitation module, a sensitive photomultiplier tube (Hamamatsu, H7732-10), and a highspeed data acquisition unit (AD Instrument, Powerlab 8/35). The 785 nm laser source operated at a 50-mW output power. The excitation beam first passed a 785 nm laser cleaner filter (Semrock, LL01-785-25) with only a 3 nm pass bandwidth. This filter removes the residual laser emission wavelength longer than 790 nm, which will cause severe background interference. Then the excitation beam was reflected by an 801nm edge dichroic beam splitter DM801LP (Semrock, FF801-Di02) and focused by a lens with a 2.5 cm focal length. The samples or rats' ears were placed around the focal plane of the lens, manipulated by a three-dimensional translation stage. Then we adjusted the position of the ear such that the laser beam focused on the major vessel. The ICG fluorescence was epi-collected by the same lens, transmitted the 801nm edge dichroic beam splitter, and passed a stack of filters to block

Biomedical Optics EXPRESS

the stray light of the excitation source. The filter sets include a 785 nm notch filter (Semrock, NF03-785E-25), an 832 nm bandpass filter 832/37 BP (Semrock, FF01-832/37-25), and two 808 nm edge long pass filters 808 LP (Semrock, BLP01-808R-25). When the bias voltage of the photomultiplier tube (PMT) increases above a threshold, the photocurrent of ICG fluorescence will appear. This output current will build up signal voltages across the resistive load on the data acquisition unit (DAQ) and be displayed on a personal computer (PC).

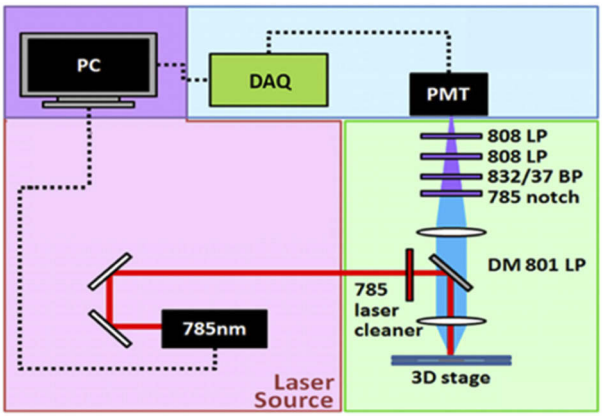

Fig. 1. Schematic diagram of a portable ICG fluorescent dosimeter. DM 801 LP: 801 nm edge dichroic beam splitter; 832/37 BP: 832 nm centered bandpass filter filters; 808 LP: 808 nm edge long-pass filters; PMT: photomultiplier tube; DAQ: data acquisition unit; PC: the personal computer.

Without laser excitation, even at a maximal bias (1V), the dark current induced signal was below the detection limit of 2 mV, indicating a light-tight condition. When we turned on the excitation laser at 50 mW, the back-scattered stray light that passed the blocking filters caused bias-dependent background signals (Fig. S1). Above the 0.8 V bias voltage, the significant background will interfere with the dosimetry. To figure out the optimal bias voltages and dynamic range for ICG dosimetry, we performed preliminary tests by injecting 1× and 0.1× clinical dosages. The peak signals right after tail-vein injection were 2.5 V (with 0.6 V bias) and 3.6 V (with 0.8 V bias), respectively. We confirmed that, within 3 V and 4 V output voltages, the output signals have a linear dependence on the ICG concentration under 0.6 V and 0.8 V bias, respectively. For 0.01× clinical dosage, the ICG fluorescence signals were comparable to the background interference from the residual excitation photons.

2.3. Preparation of ICG solution

According to the literature, the fluorescence yields of ICG below 10 µg/mL are linearly dependent on the concentration [26,27]. Considering a 70 mL/kg blood volume of a 400 g rat and a 43.7% hematocrit, the 0.5 mg/kg clinical dosage (1× dosage) corresponds to a 12.7 µg/mL concentration of dissolved ICG in circulation. This estimated *in vivo* concentration is close to the linear regime of fluorescence dosimetry. For tail-vein administration, we prepared a 200 µL bolus injection of ICG (Santa Cruz) solution with a 1 mg/mL concentration. For better solubility, the ICG solution was mixed with 20% albumin solution at a volume ratio of 1:4.

2.4. Animal model

We used N-Nitrosodiethylamine (DEN) to induce cirrhosis and liver cancer on 6 weeks old Wistar rats with 200 g weights. Four rats were divided into control, experimental group 1, and experimental group 2. One rat assigned in the control group drank normal waters. For

Biomedical Optics EXPRESS

experimental group 1 (Rat 1) and group 2 (Rat 2 and Rat 3), we feed an aqueous solution of 50 and 100 ppm (v/v) DEN (Sigma-Aldrich, St. Louis, MO, USA) daily as the sole source of drinking water for 42 days and 63 days, respectively. The DEN solution was prepared each week and consisted of an individualized dose according to the weight gain/loss of the animal. If the weight is 300-400 g, the DEN dosage would be 75 (group 1) and 150 ppm (group 2). If the weight is over 400 g, the DEN dosage would be 100 (group 1) and 200 ppm (group 2). After the DEN feeding period, rats drank normal water until 19 weeks old, which is the study's endpoint. Right before the endpoint, we performed ultrasound imaging of livers and ICG fluorescent dosimetry on the rats. Then we drew the blood for biochemical assays and sacrificed the rats for the histopathological examination of liver tissues.

2.5. Evaluate the liver lesion with the high-frequency ultrasonic imaging

The Prospect small animal ultrasound real-time image system in the experimental animal center of National Taiwan University was used for *in vivo* liver investigation. The system operated at 20 MHz acoustic frequency with a 30 μm spatial resolution. This imaging modality can non-invasively screen the presence of nodules in the rat liver. After anesthesia by Tribromoethanol (Avertin), the rat was set at dorsal decubitus. The abdominal ultrasound mode B, with a 2-D grayscale image, was applied. In addition, all parameters in the present experiment were fixed as follows: Field of view: 80%. Start of depth:3.7 mm, Acoustic intensity: 46-50 dB.

2.6. Multiphoton imaging of ICG retention after intravenous administration

Before the tail-vein injection of ICG, we used in vivo THG imaging to find the flowing blood cells and locate the corresponding blood vessel beneath the skin of a rat's ear. At a low frame rate, the THG signals of flowing blood cells will blur into a tube shape [Fig. 2(a)]. Before ICG injection, no TPF signal could be found in the region of vessels [Fig. 2(b)]. After injection (0.5 mg/kg), the TPF of ICG appeared immediately [Fig. 2(c)], reached the maximum at 1.5 minutes post-injection [Fig. 2(d)], and decayed afterward. By measuring the TPF intensity of ICG in the vessel, we could measure the time-course clearance curve of ICG.

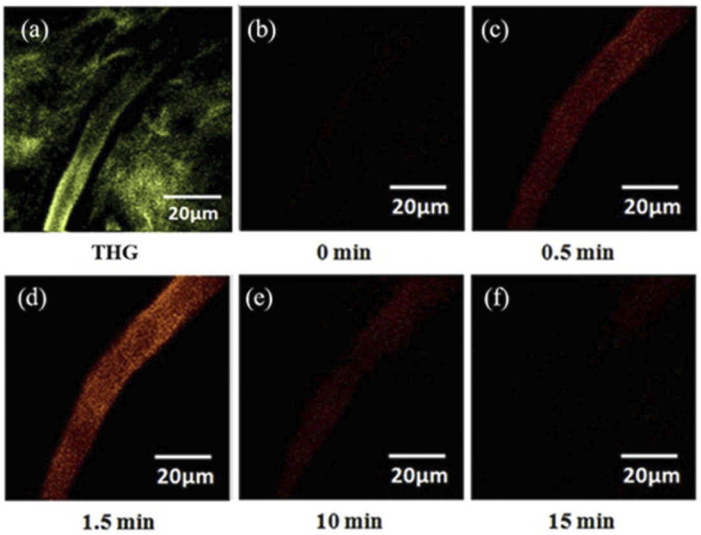

Fig. 2. *In vivo* (a) THG (green) and (b-f) TPF (red) imaging of ICG in the vessel of a rat's ear. (b) TPF image before the injection of ICG. (c-f) TPF images of intravascular ICG at the (c) 0.5 min, (d) 1.5 min, (e) 10 min, and (f) 15 min post-injection.

Biomedical Optics EXPRESS

2.7. Generate the ICG retention curve with the image processing

For the multiphoton ICG fluorescence dosimetry system, we selected a region of interest (ROI) in the TPF-image revealed vessels and calculated the average ICG fluorescence intensity by the ImageJ software. The ROI area was 5 μm × 5 μm and located in the blood vessels without touching the blood vessel walls. Then we could generate data points from each frame of time-course imaging and obtain the ICG retention curve. We modeled the retention curve using the exponential decay function $y(t)=y_0 + Aexp(-t/\tau)$, where y_0 is the constant background value, and $1/\tau$ represents the ICG clearance rate. Then we could obtain the clearance time τ of ICG after tail-vein injection. For a single-photon fluorescence dosimetry system, the ICG retention curve could be generated by the software of the data recorder.

2.8. Quantify the liver damage hallmarks

To evaluate DEN-induced liver damage, we collected 10 mL whole blood from rats and centrifuged (5 min at 1,200g, room temperature) it after being sacrificed using the cervical dislocation method. Then the damage hallmarks in serum were investigated by rat enzyme-linked immunosorbent assays. The quantified hallmarks include serum albumin, total bilirubin, glutamic pyruvic transaminase (GPT), and glutamic oxaloacetic transaminase (GOT). All the measurements were performed by the animal center of the National Taiwan University College of Medicine.

2.9. Hematoxylin-Eosin and Masson Staining for Liver Histopathology

After being sacrificed, the rat liver and tumor were removed. Those tissues were fixed in 10% formalin solution for 24 hours before the paraffin-embedded blocks were made for histopathological studies. Hematoxylin-Eosin (HE) staining and Masson staining (MS) were carried out on 5 μm sections. The staining results were imaged by Nikon Eclipse NIE microscope and evaluated by a pathologist.

2.10. Ethical statement

All rats were acclimatized in plastic cages and taken care of by the animal center. The experimental animal protocol above was approved by the National Taiwan University College of Medicine and College of Public Health Institutional Animal Care and Use Committee (IACUC) with file numbers 2012002 and 20090352. For the ICG imaging of patients' HCC liver tissues, the protocol was approved by the research ethics committee in Zhujiang Hospital, Southern Medical University (No. 2014-GDYK-008).

3. Results

3.1. Serum hallmarks reflect the liver damage by full-dose DEN feeding

The Wistar rat in the control group was healthy without any liver disease. Its serum levels of albumin, total bilirubin, GPT, and GOT were 4.1 g/dL, 0.4 mg/dL, 58.5 U/L, and 85.5 U/L, respectively. For Rat 1 in Group 1, its liver function was not seriously damaged by the reduced DEN feeding (Table S1), and neither tumor nor cirrhosis was found. For Rat 2 and Rat 3 in Group 2, serum GPT and GOT levels were significantly increased. Moreover, Rat 3 has raised bilirubin level. These biochemical assays indicate that full-dosage DEN feeding results in liver damage, while the half-dosage one does not.

3.2. Ultrasound image results of the animal model

Then we used high-frequency small animal ultrasound imaging to search tumor nodules or cirrhosis features *in vivo*. The control rat's image has a smooth reflection of the liver by the ultrasound [Fig. S2(a)]. Rat 1 has similar imaging quality of the liver, and there was no significant

Biomedical Optics EXPRESS

difference to the control group [Fig. S2(b)]. Due to severe damage, Rat 3 shows enlarged liver and non-even brightness in the liver ultrasound images (Figure S2(c)). The focal area with increased signal indicated the occurrence of cirrhosis. Interestingly, the liver of Rat 2 had a tumor sign (indicated by the yellow arrow in Figure S2(d)), but the entire liver surface was still with a relatively smooth ultra-sound reflection.

3.3. Liver lesion confirmed by H&E and Masson staining

The hematoxylin and eosin (H&E) staining can clearly distinguish the nucleus and cytoplasm to observe the cell type [28]. The blue-violet color will reveal basophilic structures, such as the nucleus, nucleic acid, and ribosome; Red, pink, or orange colors will reveal acidic structures, such as the cytoplasm. Red blood cells will present bright red, and cytoplasm will be stained into different shades of pink to fuchsia. Masson staining (MS) can distinguish between normal cells and surrounding connective tissue, which is commonly used in histology to observe the growth of collagen and to determine the degree of fibrosis [28,29]. In MS, keratin and muscle fibers reveal red, collagen and bones reveal blue or green, the cytoplasm is light red or pink, and the nucleus is dark brown. In the control group, the liver cells were evenly distributed, and the cell size was normal. Rat 1 had more dense cells surrounded by the central artery or the hepatic portal vein, but the sheath of the liver portal was still normal cells. The area of the liver portal was enlarged compared with the control group. Liver plates are arranged neatly without pseudolobules. For Rat 3, in addition to the dense aggregation of cells around the blood vessels, the sheath had a significantly filamentous extension of the fiber into the hepatocytes and fibrosis (red, Fig. S3). And the liver cell areas were extremely uneven, which indicated the liver plate system rearranged. Pseudolobular patterns were observed (Fig. S4), representing severe liver cirrhosis. For Rat 2, non-tumor regions showed regenerated hepatocytes. Fibrosis was widely present in the liver (Fig. S5), but this type of fibrosis preserves better liver function. These biochemical assays of serum, *in vivo* ultrasound images, and histopathological images above conclude our DEN-feeding rat model successfully induced liver cancer and cirrhosis.

3.4. Validate change of liver function by multiphoton dosimetry of ICG fluorescence

Then we administered a bolus of ICG through the tail-vein of rats for multiphoton fluorescence dosimetry. We want to check whether the ICG leaks into tissues or not. In the control rat, the fluorescence intensity decayed below 10% within 15 minutes [Fig. 3(b)]. Fitted by the single exponential decay formula $y(t)=y_0 + Aexp(-t/\tau)$, the curve [red curve in Fig. 3(b)] has $y_0 = 3.88$, $A = 127.42$, and $\tau = 4.46$ minutes (Table S2). Rat 1 also has a fast clearance of ICG [red curve in Fig. 3(c)] with $\tau = 3.82$ minutes. In contrast, liver cancer in Rat 3 slowed down the ICG metabolism [green curve in Fig. 3(c)] and increased the retention time to 13.9 minutes (Table S2). The corresponding ICG-R15 is above 40%. For Rat 2, even though it has high GPT/GOT serum levels and a tumor nodule in the liver's ultrasound image, it still maintains a good clearance rate as that of the control rat.

3.5. In vivo measurement of the ICG retention curve with 785 nm laser

After validating that ICG fluorescence decay could report the alteration of liver function by liver cancer, we built up a 785 nm laser-based ICG fluorescence dosimeter as a portable system for clinical use. From the 785 nm excited ICG fluorescence spectra, we confirmed the fluorescence dosimetry is linear at concentrations below 10 μg/mL (Fig. S6). The 14 μg/mL data point showed an efficiency saturation, which agrees with the literature [26,27]. Since the 1× dosage is already at the saturation edge, we first investigated whether we could use a lower dosage of ICG to achieve liver function evaluation. In humans, over 90% ICG in blood could be metabolized and cleared within 15 minutes [30]. We used 1 and 1/10 times of the clinic dosage to administer ICG in healthy rats. With the excitation output power of 50 mW, PMT voltage value of 0.4V, the

Biomedical Optics EXPRESS

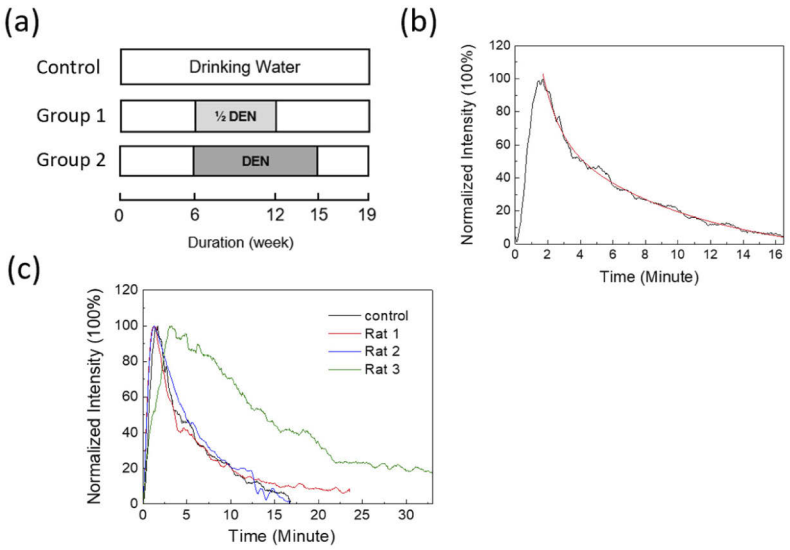

Fig. 3. (a) Experimental protocols of DEN feeding by weeks for rat liver lesion model. Group 1 was fed by a half dose of DEN compared with Group 2. The 19th week is the endpoint of studies. (b) The retention curve of normalized ICG fluorescence in the vessels of the control rat (black curve). We use single exponential decay to fit the data (red curve). (c) Comparison of the retention curves of ICG in different Rats.

background signal was from 0.15 to 0.17 volts. Since the hemoglobin has a higher absorption constant than extravascular matrices, we could identify the region with blood vessels by the variation of back-scattered 785 nm signals. The retention curves for both dosages are measurable, and as we expected, they all presented 10% ICG-R15 (Fig. 4). Fitted by a single exponential decay model $y(t)=y_0 + Aexp(-t/\tau)$, the corresponding lifetime is on average 4.560 minutes for rats with 1× ICG and 4.759 minutes for rats with 0.1× ICG (Table S3). The decay time τ could serve as a quantitative index to evaluate the liver's metabolic function.

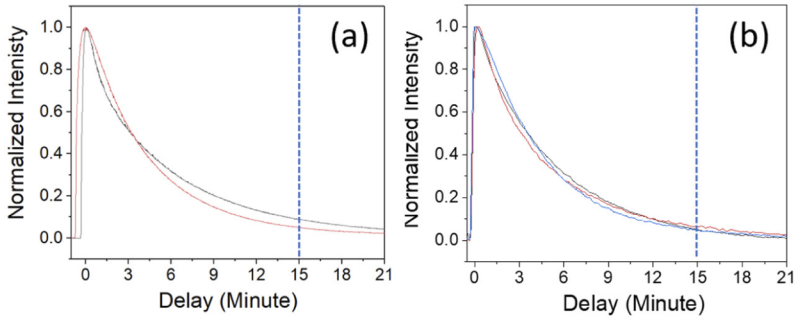

Fig. 4. The ICG retention curves of (a) 1× (2 rats) and (b) 0.1× (3 rats) clinical ICG dosage (1× = 0.5 mg/kg). PMT voltage was 0.6 volts and 0.8 Volt, respectively.

4. Discussion

Except for aggregation-induced quantification error, some other physiological conditions may affect the correctness of liver function evaluation. The factors include the serum bilirubin level,

Biomedical Optics EXPRESS

the hepatic blood flow [31], the cirrhosis-induced hepato-splanchnic hypoperfusion [31,32], and the accumulation of ICG in cholestasis regions of the well-differentiated HCC (Fig. S7). Besides, the iodine in the formula compound of ICG may cause an allergy [33]. Even so, the integration of the ICG-R15 test with the MELD score can still increase the accuracy of survival prediction than using the MELD score alone [34]. Thus, the ICG-R15 tests still attract clinicians to better predict liver failure after liver resection, especially in HCC patients with cirrhosis [35].

Here, we exploit the advantages of non-invasiveness and low background interference of ICG fluorescence dosimetry to evaluate liver function reserve. This approach can avoid the psychological stress caused by multiple blood sampling and reduce the artificial effects. It is also possible to predict the 15-minute retention level of ICG at the 3-4 minutes after injection. In addition, our method reduces the dosage of ICG, which is expensive, and the iodine may cause an allergic reaction in some patients with iodine allergies. Our results demonstrate that 1/10 clinical dosage is possible to evaluate liver function.

Then we apply this ICG fluorescence dosimetry in the HCC animal model. We found that rat 3 in the HCC condition has an ICG-R15 higher than 40%. That prolonged ICG circulation indicates an insufficient capacity of liver metabolism. Its liver showed an apparent tumor nodule in the high-frequency ultrasound image [Fig. S2(d)]. The architectural distortion and pseudolobules formation appeared in the histopathology images [Fig. S4(c) & 4(d)]. In contrast to rat 3, both half-dosage rat 1 and full-dosage rat 2 have similar ICG decay time (4-5 minutes) to control rats. HCC rat 2 still has a normal liver function because the liver has less severe fibrosis and a smaller tumor area [See Fig. S2(c) and S5]. These pieces of evidence support the notion that the ICG fluorescence dosimetry can reflect the degraded function reserve in the HCC liver. With more pre-clinical and clinical validation, we believe the 785 nm excited single-photon fluorescence dosimeter of circulated ICG can quickly assess the ICG retention right after the administration and help the medical doctors to decide the patient's liver function reserve.

Funding. The Science and Technology Development Fund, Macau SAR (File no. 0011/2019/AKP, 0026/2021/A, 0120/2020/A3, 018/2017/A1, 122/2016/A3); Research Services and Knowledge Transfer Office, University of Macau (MYRG2019-00022-FHS); National Health Research Institutes (NHRI-EX101-9936EI); National Science Council, Taiwan (NSC 100-2628-E-002-006).

Acknowledgments. The authors would like to thank the help from the animal facility of the Faculty of Health Sciences, University of Macau, and the Molecular Imaging Center, National Taiwan University.

Disclosures. The authors declare no conflict of interest.

Data Availability. The data that support the findings of this study are available from the corresponding author upon reasonable request.

Supplemental document. See Supplement 1 for supporting content.

References

1. D. Galun, D. Basaric, M. Zuvela, P. Bulajic, A. Bogdanovic, N. Bidzic, and M. Milicevic, "Hepatocellular carcinoma: From clinical practice to evidence-based treatment protocols," World J. Hepatol. **7**(20), 2274 (2015).
2. H. Xu and Y. Mao, "A brief comment on liver resection for hepatocellular carcinoma," Gastroenterology Report **1**(3), 184–185 (2013).
3. R. N. Pugh, I. M. Murray-Lyon, J. L. Dawson, M. C. Pietroni, and R. Williams, "Transection of the oesophagus for bleeding oesophageal varice," Br. J. Surg. **60**(8), 646–649 (2005).
4. J. M. Llovet, J. Bruix, and G. J. Gores, "Surgical resection versus transplantation for early hepatocellular carcinoma: clues for the best strategy," Hepatology (Hoboken, NJ, U. S.) **31**(4), 1019–1021 (2000).
5. F. Durand and D. Valla, "Assessment of the prognosis of cirrhosis: Child–Pugh versus MELD," J. Hepatol. **42**(1), S100–S107 (2005).
6. E. Cholongitas, G. Papatheodoridis, M. Vangeli, N. Terreni, D. Patch, and A. K. Burroughs, "Systematic review: the model for end-stage liver disease–should it replace Child-Pugh's classification for assessing prognosis in cirrhosis?" Aliment. Pharmacol. Ther. **22**(11-12), 1079–1089 (2005).
7. F. Lu, F. Wu, P. Hu, Z. Peng, and D. Kong, "Automatic 3D liver location and segmentation via convolutional neural network and graph cut," Int. J. Comput. Assist. Radiol. Surg. **12**(2), 171–182 (2017).

Biomedical Optics EXPRESS

8. Z. P. Zhou, L. L. Long, W. J. Qiu, G. Cheng, L. J. Huang, T. F. Yang, and Z. K. Huang, "Evaluating segmental liver function using T1 mapping on Gd-EOB-DTPA-enhanced MRI with a 3.0 Tesla," BMC Med. Imaging **17**(1), 20 (2017).
9. Q. Lu, W. Ling, C. Lu, J. Li, L. Ma, J. Quan, D. He, J. Liu, J. Yang, T. Wen, H. Wu, H. Zhu, and Y. Luo, "Hepatocellular carcinoma: stiffness value and ratio to discriminate malignant from benign focal liver lesions," Radiology (Oak Brook, IL, U. S.) **275**(3), 880–888 (2015).
10. H. J. Kim, C. Y. Kim, Y. H. Hur, Y. S. Koh, J. C. Kim, C. K. Cho, and H. J. Kim, "Comparison of remnant to total functional liver volume ratio and remnant to standard liver volume ratio as a predictor of postoperative liver function after liver resection," Korean J. Hepatobiliary Pancreat. Surg. **17**(4), 143–151 (2013).
11. T. Chapelle, B. O. De Beeck, I. Huyghe, S. Francque, A. Driessen, G. Roeyen, D. Ysebaert, and K. De Greef, "Future remnant liver function estimated by combining liver volumetry on magnetic resonance imaging with total liver function on 99mTc-mebrofenin hepatobiliary scintigraphy: can this tool predict post-hepatectomy liver failure?" HPB **18**(6), 494–503 (2016).
12. S. Heyman, "Hepatobiliary scintigraphy as a liver function test," J. Nucl. Med. **35**(3), 436–437 (1994).
13. S. Matsuzaki, M. Onda, T. Tajiri, and D. Y. Kim, "Hepatic lobar differences in progression of chronic liver disease: correlation of asialoglycoprotein scintigraphy and hepatic functional reserve," Hepatology (Hoboken, NJ, U. S.) **25**(4), 828–832 (1997).
14. W. De Graaf, R. L. Veteläinen, K. de Bruin, A. K. van Vliet, T. M. van Gulik, and R. J. Bennink, "^{99m}Tc-GSA scintigraphy with SPECT for assessment of hepatic function and functional volume during liver regeneration in a rat model of partial hepatectomy," J. Nucl. Med. **49**(1), 122–128 (2008).
15. M. Sakoda, S. Ueno, S. Iino, K. Hiwatashi, K. Minami, Y. Kawasaki, H. Kurahara, Y. Mataki, K. Maemura, and Y. Uenosono, "Anatomical laparoscopic hepatectomy for hepatocellular carcinoma using indocyanine green fluorescence imaging," J. Laparoendosc. Adv. Surg. Tech. A. **24**(12), 878–882 (2014).
16. J. T. Alander, I. Kaartinen, A. Laakso, T. Pätilä, T. Spillmann, V. V. Tuchin, M. Venermo, and P. Välisuo, "A review of indocyanine green fluorescent imaging in surgery," Int. J. Biomed. Imaging. **2012**, 1 (2012).
17. L. Boni, G. David, A. Mangano, G. Dionigi, S. Rausei, S. Spampatti, E. Cassinotti, and A. Fingerhut, "Clinical applications of indocyanine green (ICG) enhanced fluorescence in laparoscopic surgery," Surg. Endosc. **29**(7), 2046–2055 (2015).
18. Y. Watanabe and K. Kumon, "Assessment by pulse dye-densitometry indocyanine green (ICG) clearance test of hepatic function of patients before cardiac surgery: its value as a predictor of serious postoperative liver dysfunction. Journal of cardiothoracic and vascular anesthesia," Journal of Cardiothoracic and Vascular Anesthesia **13**(3), 299–303 (1999).
19. Y. Y. Wang, X. H. Zhao, L. Ma, J. Z. Ye, F. X. Wu, J. Tang, X. M. You, B. D. Xiang, and L. Q. Li, "Comparison of the ability of Child-Pugh score, MELD score, and ICG-R15 to assess preoperative hepatic functional reserve in patients with hepatocellular carcinoma," J. Surg. Oncol. **118**(3), 440–445 (2018).
20. M. S. Alfano, S. Molfino, S. Benedicenti, B. Molteni, P. Porsio, E. Arici, F. Gheza, M. Botticini, N. Portolani, and G. L. Baiocchi, "Intraoperative ICG-based imaging of liver neoplasms: a simple yet powerful tool: preliminary results," Surg. Endosc. **33**(1), 126–134 (2019).
21. T. Iijima, T. Aoyagi, Y. Iwao, J. Masuda, M. Fuse, N. Kobayashi, and H. Sankawa, "Cardiac output and circulating blood volume analysis by pulse dye-densitometry," J. Clin. Monit. **13**(2), 81–89 (1997).
22. A. De Gasperi, E. Mazza, and M. Prosperi, "Indocyanine green kinetics to assess liver function: Ready for a clinical dynamic assessment in major liver surgery?" World J. Hepatol. **8**(7), 355–367 (2016).
23. R. B. Dorshow, J. E. Bugaj, B. D. Burleigh, J. R. Duncan, M. A. Johnson, and W. B. Jones, "Noninvasive fluorescence detection of hepatic and renal function," J. Biomed. Opt. **3**(3), 340–346 (1998).
24. R. Weigand, F. Rotermund, and A. Penzkofer, "Aggregation dependent absorption reduction of indocyanine green," J. Phys. Chem. A **101**(42), 7729–7734 (1997).
25. P.-C. Wu, T.-Y. Hsieh, Z.-U. Tsai, and T.-M. Liu, "In vivo quantification of the structural changes of collagens in a melanoma microenvironment with second and third harmonic generation microscopy," Sci. Rep. **5**(1), 8879 (2015).
26. R. W. Flower and B. F. Hochheimer, "Quantification of indicator dye concentration in ocular blood vessels," Exp. Eye Res. **25**(2), 103–111 (1977).
27. R. Benson and H. A. Kues, "Fluorescence properties of indocyanine green as related to angiography," Phys. Med. Biol. **23**(1), 017159–163 (1978).
28. A. T. Feldman and D. Wolfe, "Tissue processing and hematoxylin and eosin staining," Methods Mol. Biol. **1180**, 31–43 (2014).
29. P. S. Chen, Y. P. Li, and H. F. Ni, "Morphology and evaluation of renal fibrosis," Adv. Exp. Med. Biol. **1165**, 17–36 (2019).
30. J. Zheng, W. Xie, Y. Huang, Y. Zhu, and L. Jiang, "The technique of 3D reconstruction combining with biochemistry to build an equivalent formula of indocyanine green (ICG) clearance test to assess the liver reserve function," BMC Surg. **20**(1), 283 (2020).
31. L. Lau, C. Christophi, M. Nikfarjam, G. Starkey, M. Goodwin, L. Weinberg, L. Ho, and V. Muralidharan, "Assessment of liver remnant using ICG clearance intraoperatively during vascular exclusion: early experience with the ALIIVE technique," HPB Surg. **2015**, 1 (2015).

Biomedical Optics EXPRESS

32. P. Koranda, M. Myslivecek, J. Erban, V. Seidlová, and V. Husák, "Hepatic perfusion changes in patients with cirrhosis: Indices of hepatic arterial blood flow," Clin. Nucl. Med. **24**(7), 507–510 (1999).
33. P. Ott, S. Keiding, and L. Bass, "Intrinsic hepatic clearance of indocyanine green in the pig: dependence on plasma protein concentration," Eur. J. Clin. Invest. **22**(5), 347–357 (1992).
34. J. J. Vos, K. Wietasch, A. R. Absalom, H. G. Hendriks, and T. W. Scheeren, "Green light for liver function monitoring using indocyanine green? An overview of current clinical applications," Anaesthesia **69**(12), 1364–1376 (2014).
35. Q. S. Sheng, R. Lang, Q. He, Y. J. Yang, D. F. Zhao, and D. Z. Chen, "Indocyanine green clearance test and model for end-stage liver disease score of patients with liver cirrhosis," Hepatobiliary Pancreat. Dis. Int. **8**(1), 46–49 (2009).